Excitonic characteristics of blue-emitting quantum dot materials in group II-VI using hybrid time-dependent density functional theory

Pingping Han,[1] Jingjing Min,[1] Zaiping Zeng,[1,*] Christos S. Garoufalis,[2,†] Sotirios Baskoutas,[2] Yu Jia,[1,3,‡] and Zuliang Du[1]

[1]*Key Laboratory for Special Functional Materials of Ministry of Education, Collaborative Innovation Center of Nano Functional Materials and Applications, and School of Materials Science and Engineering, Henan University, Kaifeng, Henan 475001, China*

[2]*Materials Science Department, University of Patras, 26504 Patras, Greece*

[3]*International Laboratory for Quantum Functional Materials of Henan, and School of Physics and Engineering, Zhengzhou University, Zhengzhou, Henan 450001, China*

(Received 14 May 2021; revised 17 June 2021; accepted 24 June 2021; published 6 July 2021)

Colloidal quantum dots (QDs) of group II-VI are key ingredients of next-generation QD light-emitting diodes technology for display and lighting, yet the understanding of their luminescent characteristics are far from being mature. Using a hybrid time-dependent density functional theory, we have studied the electronic and excitonic properties of blue-emitting colloidal QDs within group II-VI containing a thousand atoms or more, including CdSe, CdS, ZnSe, and ZnS QDs, considering both quantum confinement and surface ligand effects. It is found that the calculated optical gaps are in excellent quantitative agreement with experiment, irrespective of the QD nature. Scaling laws of size-dependent energy gaps governed solely by quantum confinement effects have further been explored at both single-particle level and correlated excitonic level for all QDs. With concurrently stoichiometric control and enhancing quantum confinement effects, we have predicted an unusual switching of symmetry character of the highest occupied molecular orbital state from a Γ_3 to a Γ_1 symmetry at ultrasmall size ($\sim$1 nm) for all QDs. After the switching, pronounced linearly polarized band-edge excitonic emission is activated. The radiative exciton decay lifetime is found to increase monotonically with increasing the QD size and tends to saturate at larger sizes. Finally, we have explored the surface passivation mechanism of inorganic chloride ligand, and identified various favorable Cd-Cl bonding configurations which enable an effective surface passivation resembling the commonly applied pseudohydrogen passivation scheme. We find that chloride ligand serves as a hole delocalization ligand and tends to redshift the absorption spectra, reduce the absorption intensity, and significantly enhance the exciton decay lifetime. Our results provide a guideline for spectroscopic studies of excitonic characteristics of colloidal QDs within group II-VI.

DOI: 10.1103/PhysRevB.104.045404

I. INTRODUCTION

Colloidal quantum dots (QDs) have demonstrated their great potential in modern light-emitting devices owing to their high stability, tunable emission spectrum, narrow bandwidth, and broad luminescent spectral range [1–3]. Comparing with traditional display technology, QD based light-emitting diodes technology has been demonstrated to be superior in terms of color saturation and gamut, processing cost, and power consumption, and has been considered to be one of most promising candidates for the next generation of display and lighting [4–6]. With nearly two decades' engagement, QD light-emitting diodes have experienced tremendous development, with both brightness and external quantum efficiency rivaling the state-of-the-art organic light-emitting devices [2,3]. Light-emitting devices based on QDs of group II-VI, including those of CdSe, CdS, ZnSe, and ZnS, represent one of the most well-developed technologies, being at the frontier towards commercialization. Among the three primary-color devices, the efficiency and operational lifetime of blue devices are inferior to their green and red counterparts, therefore limiting their application to full-color display and ultimately towards lighting [7–10]. The associated reasons from the fundamental physics point of view are tightly bound to the intrinsic electronic, surface, and optical properties of blue QDs. Indeed, blue QDs exhibit considerable larger band gaps and consequently smaller sizes comparing with those green and red counterparts, which increase the energy loss pathways of exciton quenching. Controlling of the surface physics or chemistry of small-size blue QDs towards defect-free QDs is experimentally challenging. This otherwise leads to poor photo- and thermal stability of the synthesized QDs, preventing a reliable experimental characterization of their excitonic optical properties, which is particularly true for ZnSe QDs [3,11–13]. Moreover, the development of blue light-emitting devices has involved a diverse variety of QD candidate materials, particularly including CdSe [14], CdS [2,15], and ZnSe-based QDs [3,13] of group II-VI. However, it remains elusive how and to what extent the luminescence characteristics of those candidate QD materials differ from each other.

From a theoretical point of view, study of excitonic properties of semiconductor QDs can be performed at different levels of theory. Solving the Bethe-Salpeter equation on top of *GW* calculations represents the state-of-the-art methods

*zaiping.zeng@henu.edu.cn
†garoufal@upatras.gr
‡jiayu@henu.edu.cn

in terms of accuracy at both cluster and infinite-bulk limits. However, it is computationally highly demanding, and imposes significantly practical limits on the QD size (usually <100 atoms for confined systems) and complexity. The continuum models, such as effective-mass approximation and multiband $\mathbf{k}\cdot\mathbf{p}$ methods, are best suited for QDs within the weak confinement regime, but fails where atomistic effects become important. Empirical or semiempirical methods, such as tight-binding model [16–18] and empirical pseudopotential method [19–23], combined with the screened configuration interaction with a selected screening model, can treat QDs up to millions' atoms. However, those methods are heavily parametrized and usually rely on a predefined unrelaxed geometry. Moreover, due to the lack of total energy calculations, surface ligands effects, as supposed to be highly important for colloidal QDs considered herein, remain challenging to be explicitly considered. Therefore, an accurate description of the excited-state properties of QDs taking into account the size and surface ligand effects is highly appealing, considering the largely enhanced excitonic effects associated with the three-dimensional confinement effects and reduced screening.

In this contribution, we provide a full *ab initio* treatment of excitonic properties of colloidal QDs with realistic sizes containing a thousand atoms or more. The electronic structures are calculated using density functional theory with B3LYP hybrid functional. On top of the ground-state calculations, time-dependent density functional theory is subsequently applied to account for the many-body excitonic effects. Such a hybrid time-dependent density functional theory has been successfully applied on the study of excitonic properties of QDs within group III-V [24]. The emphasis is placed on the technologically important blue emitting QD materials of group II-VI, including those of CdSe, CdS, ZnSe, and ZnS, considering both quantum confinement and surface ligand effects. We have determined a variety of excitonic optical properties of those QDs, including size-dependent single-particle and optical gaps, exciton decay lifetime, singlet-triplet splitting, and optical absorption spectra. We first discuss the electronic structure evolution of the electronic states when going from bulk to QD regime, considering both stoichiometric and off-stoichiometric QDs, and describe the resulted exciton fine structure obtained from the current hybrid density functional theory. We then explore the size-dependent excitonic properties of those group II-VI QDs by considering solely quantum confinement effects. Scaling laws of size-dependent excitonic properties have been explored. Finally, we study the surface ligand effects by introducing the simple inorganic chloride ligand, which has been recently introduced within a postsynthetic ligand exchange process to boost performance of the blue-emitting QD device [3]. We have explored the corresponding surface passivation scheme and identified its impact on the excitonic properties of those group II-VI QDs. In the following section, we will outline the computational details. Thereafter, in Sec. III, numerical results and related discussion are presented. Section IV is devoted to conclusions.

II. COMPUTATIONAL DETAILS

The quantum dots (QDs) are cut from the corresponding bulk materials with nearly spherical shape (i.e., characterized by diameter D) of zinc-blende structure. Two types of QDs are considered, i.e., stoichiometric and cation-rich nonstoichiometric QDs. The former type of QD is centered on the center of mass and exhibits a C_{3v} point group symmetry, while the latter one is centered on a cation atom and has a T_d point group. The QD size ranges from approximately 1 nm to 4 nm, depending on the QD nature, which corresponds to the total number of atoms ranging from 65 atoms to 1360 atoms, and therefore within the strong confinement regime. QDs of those sizes can be synthesized using the sophisticated modern colloidal fabrication method [25–27]. For ideal pseudohydrogen passivation, if not otherwise stated, the surface dangling bonds of cations and anions are saturated with pseudohydrogen atoms with modified charges of 1.5 and 0.5, respectively.

All calculations are performed with the Turbolmole suite of programs [28]. The geometry optimization is performed in the framework of density functional theory (DFT) with generalized gradient approximation (GGA) of Perdew-Burke-Ernzerhof (PBE) type [29], which is known to predict rather accurately the structural properties. However, this level of theory is known to underestimate the band gap and is detrimental for the modeling of optical properties. We therefore employ the hybrid nonlocal exchange-correlation functional of Becke and Lee, Yang and Parr (B3LYP [30]) to calculate reliably the single-particle highest occupied molecular orbital–lowest unoccupied molecular orbital (HOMO-LUMO) gap. We have chosen a basis set of double zeta quality (namely, the def2-SVP basis sets of the Karlsruhe group [31,32]) throughout the work, which allows for calculations of systems with thousands of atoms without significantly compromising the accuracy (<0.1 eV), thanks to the employment of point-group theory and high-performance computing facilities. The excitonic optical properties are calculated on top of the B3LYP results, using the linear-response time-dependent DFT (TDDFT). We note that the energy of the lowest symmetry-allowed and spin allowed transition (singlet state) is considered as the optical gap regardless of its oscillator strength. The radiative decay lifetime (τ_X) is calculated according to [33,34], $\frac{1}{\tau_X} = \frac{4\alpha E_X n |M_X|^2}{m_0^2 \hbar c^2}$, where n is the refractive index, α is the fine-structure constant, m_0 is the electron rest mass, c is the velocity of light, E_X is the exciton energy, and M_X is the electric dipole transition matrix element obtained from the TDDFT calculations. We note that this formula derived within the effective-mass approximation is considerably simplified compared to a truly microscopic description of radiative lifetimes. It involves the refractive index of the bulk material, and the resulted radiative lifetime may be underestimated. The singlet-triplet splitting is defined as the energy difference between the lowest singlet and triplet states based on the optimized ground-state geometry. For symmetry analysis, Kosters' notations of single group symmetry representations have been employed.

III. NUMERICAL RESULTS AND DISCUSSION

A. Exciton fine structure

Prior to the presentation of numerical results, we first describe the evolution of the electronic states when going from bulk to QD, which is established from the hybrid density

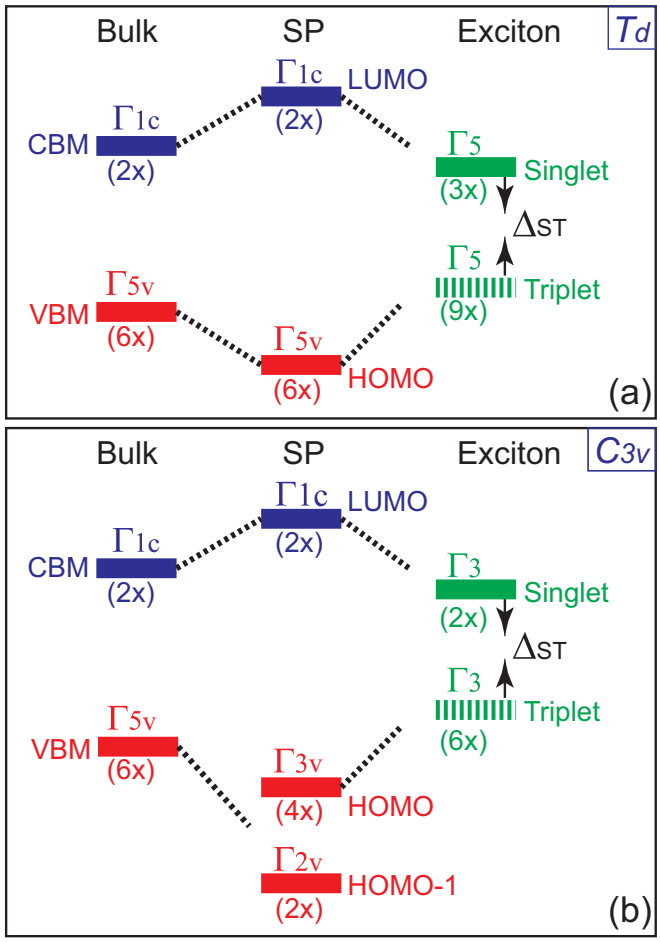

FIG. 1. (a), (b) Symmetry characters of valence band maximum (VBM) and conduction band minimum (CBM) in group II-VI bulk material (left column), the HOMO and LUMO states of the corresponding (a) nonstoichiometric (T_d point group) and stoichiometric (C_{3v} point group) quantum dots considered herein at the single-particle (SP) level obtained by the DFT/B3LYP method (central column), and the resulted exciton manifolds obtained from TDDFT calculations (rightmost column). The degeneracy of the energy levels or exciton manifolds is shown in the parentheses. In the rightmost column, a thick solid horizontal line indicates a symmetry allowed and spin allowed exciton state (singlet state) and a thick dashed horizontal line indicates a symmetry allowed but spin-forbidden exciton state (triplet state). The spin-orbit interaction is neglected but the exchange interaction is considered.

functional theory. Bulk materials of group II-VI stabilized with zinc-blende structure, i.e., CdSe, CdS, ZnSe, and ZnS as we considered herein, are known to be direct-gap ionic semiconducting materials and have a T_d point group symmetry. The corresponding valence band maximum (VBM) is contributed nearly purely from the p orbital of anion atoms and has a Γ_{5v} symmetry and the conduction band minimum (CBM) is derived from the s orbital of cation atoms and has a Γ_{1c} symmetry (cf. Fig. 1). The s-p coupling, that forms the bonding-antibonding states, leads to the opening of the electronic gap. This remains true when going from bulk to QD regime. In QD regime, we find that the average bond length of optimized QD interior atoms obtained at the GGA/PBE level of theory remains nearly identical to that of their bulk counterpart, irrespective of QD size, QD nature, and stoichiometry. For example, the average Cd-Se bond length ranges from 2.679 Å to 2.692 Å for CdSe QDs with total atoms being from less than 100 to over 1000 and is nearly identical to their bulk counterpart (∼2.682 Å).

When cutting a QD from the corresponding bulk parentage, the highest point-group symmetry for colloidal QDs with zinc-blende structure is T_d, and those QDs are usually off stoichiometric. The symmetry characters of the corresponding highest occupied molecular orbital (HOMO) state and lowest unoccupied molecular orbital (LUMO) state resemble their bulk counterpart, having Γ_{5v} and Γ_{1c} symmetries, respectively [cf. Fig. 1(a)]. However, with stoichiometric control, the point-group symmetry of the QD can be lowered to C_{3v}. This results in the split of sixfold-degenerate Γ_{5v} states into a fourfold Γ_{3v} state at a higher energy being the HOMO state, and a twofold Γ_{2v} state at a lower energy [cf. Fig. 1(b)]. We find that the lowest exciton state has a nearly pure contribution from the HOMO → LUMO transition for all QDs considered herein. The corresponding symmetry character can thus be obtained from the direct product of the single-particle electron and hole states involved in the transition. It is found that the lowest exciton manifold of off-stoichiometric QDs with T_d point group symmetry consists of a ninefold degenerate, optically passive ("dark") spin-triplet state at a lower energy and a threefold, circularly polarized, optically active ("bright") spin-singlet state at a higher energy [cf. Fig. 1(a)], while, for stoichiometric QDs with C_{3v} point group symmetry, the lowest exciton manifold typically consists of a sixfold degenerate dark spin-triplet state at a lower energy and threefold degenerate, in-plane polarized bright exciton state at a higher energy [cf. Fig. 1(b)].

B. Size effects

Keeping the exciton fine structure in mind, we next examine the electronic and optical gaps of those blue-emitting QDs using both DFT/B3LYP and TDDFT@DFT/B3LYP. At the former single-particle level of theory, the excitonic effects are neglected, and they are properly accounted for at the latter correlated excitonic level of theory. The size-dependent electronic and optical gaps for all QD material systems are shown in Fig. 2. It is found that the electronic gaps of all QDs obtained from the current hybrid DFT are systematically larger than that of their bulk counterparts, irrespective of QD size, QD nature, and stoichiometry, as expected from the quantum confinement effects. This cannot always be reached from the DFT point of view considering the fact that LDA and GGA functionals predict electronic gaps being much smaller than experiment even in bulk phase. Furthermore, the application of TDDFT on top of DFT calculations using those LDA and GGA functionals often ends with the well-known "negative exciton binding" issue, that is, the optical gap obtained at the correlated exciton level appears much larger than the uncorrelated single-particle gap [45]. In contrast, when accounting for the excitonic effects employing the current hybrid TDDFT scheme, the optical gaps appear systematically lower than the electronic gaps, giving a physically consistent picture. Moreover, the calculated optical gaps are found to be in excellent

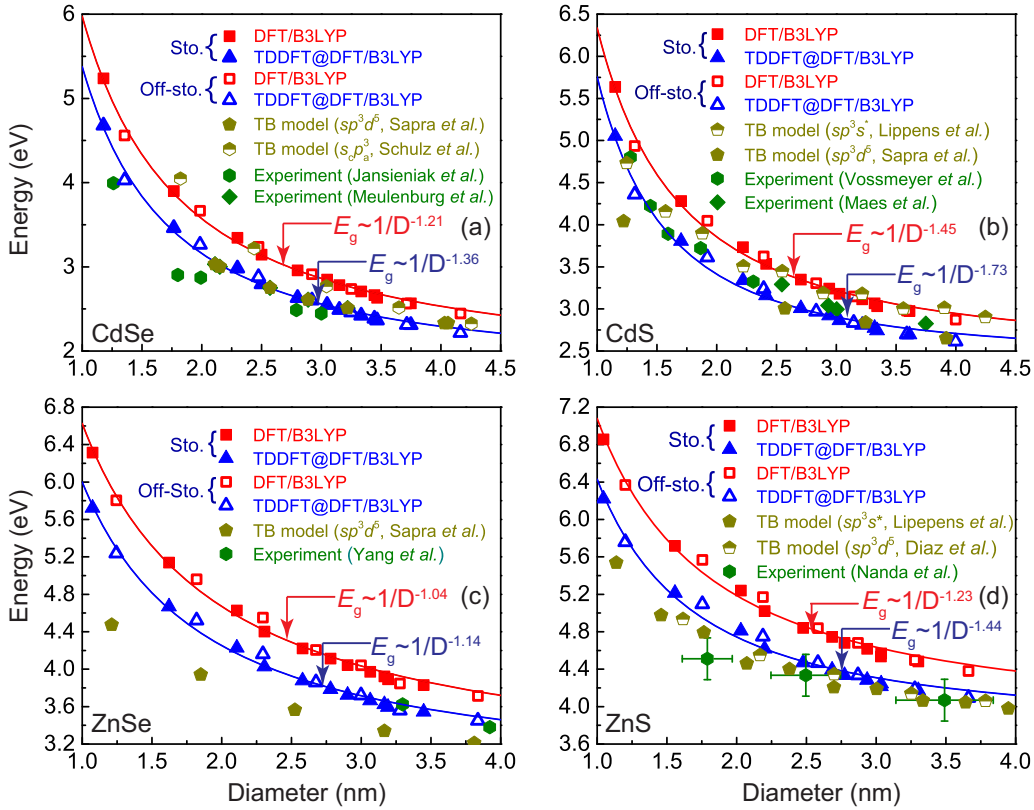

FIG. 2. Electronic and optical gaps of stoichiometric and off-stoichiometric (a) CdSe, (b) CdS, (c) ZnSe, and (d) ZnS quantum dots as a function of the dot size obtained using DFT/B3LYP and TDDFT@DFT/B3LYP levels of theory, respectively. Each solid line represents a fit according to Eq. (1). The calculated results are compared with available experimental measurements [35–40] and theoretical data based on various tight binding (TB) models [41–44].

agreement with experiments for all QD material systems and realistic QD sizes across a wide range [cf. Figs. 2(a)–2(d)].

The electronic gap is known to scale as $E_g \propto 1/D^2$ using a particle-in-box model within the single-band isotropic effective-mass approximation [46]. Considering such a scaling law, and for ease of comparison with commonly available experimental measurements or theoretical results based on other methods, we fit the calculated gaps as a function of dot size according to the following analytical formula:

$$E_g = E_{g,\text{bulk}} + \alpha/D^{\gamma}, \tag{1}$$

where $E_{g,\text{bulk}}$ is the electronic or optical gap at the bulk limit, which is taken from the experimental value [35–40] (cf. Table I), α is a proportionality constant, and γ is a real number. The resultant fitting parameters for all QD systems are compiled in Table I. We find that the obtained α value decreases with increasing band gap energy of the bulk material with α_{CdSe} being the largest, while α_{ZnS} is the smallest. The γ value obtained for all QD materials differ significantly from 2, as expected from a simple single-band effective-mass approximation using a particle-in-box model [46]. The excitonic effects are found to be important. They tend to decrease α and increase γ for all QD material systems, thus "softening" the size-dependent scaling of the gaps.

For CdSe QDs, the scaling of the size-dependent electronic gap obtained using the hybrid density functional theory appears in excellent quantitative agreement with experiment obtained from the photoemission measurement

TABLE I. Obtained fitting parameters α and γ for CdSe, CdS, ZnSe, and ZnS quantum dots. The bulk electronic gap $E_{g,\text{bulk}}$ (in units of eV) is taken from the experimental value measured at cryogenic temperature. The optical gap $E^X_{g,\text{bulk}}$ (in units of eV) is obtained by subtracting the bulk exciton binding energy from the corresponding electronic gap. The error bars are introduced by allowing 5% fluctuation in the experimental energy gaps used in the fitting process.

	Band gap (eV)			Optical gap (eV)		
Materials	$E_{g,\text{bulk}}$	α	γ	$E^X_{g,\text{bulk}}$	α^X	γ^X
CdSe	1.74	4.24 ± 0.05	1.21 ± 0.06	1.725	3.64 ± 0.05	1.36 ± 0.09
CdS	2.42	3.92 ± 0.06	1.45 ± 0.13	2.405	3.35 ± 0.04	1.73 ± 0.2
ZnSe	2.82	3.81 ± 0.11	1.04 ± 0.08	2.802	3.20 ± 0.11	1.14 ± 0.11
ZnS	3.78	3.30 ± 0.16	1.23 ± 0.17	3.76	2.67 ± 0.15	1.44 ± 0.27

[$E_g = 1.74 + 4.11/D^{1.1}$ (Ref. [36])], and with semiempirical pseudopotential calculations, i.e., $E_g \propto 1/D^{1.18}$ [cf. Table I and Fig. 2(a); see Ref. [47]]. When accounting for excitonic effects using TDDFT, the scaling of a size-dependent optical gap is found to nearly perfectly agree with experiment, i.e., $E_g^X \propto 1/D^{1.38}$ [cf. Table I and Fig. 2(a); see Refs. [35,36]]. Comparing with CdSe QDs, the scaling for CdS QDs becomes softer, delivering $\gamma_{\mathrm{CdS}} = 1.45$ and $\gamma_{\mathrm{CdS}}^X = 1.73$, respectively. This is again in good agreement with experiment obtained from the optical absorption measurement, i.e., $E_g^X = 2.39 + 3.48/D^{1.64}$ [cf. Table I and Fig. 2(b); see Refs. [37,38]].

While considerable studies are available on the electronic and excitonic properties of Cd-containing QDs, significantly fewer have been focused on environmentally friendly Cd-free QDs of group II-VI. This can, to a large extent, be attributed to the instability nature of the experimentally synthesized QDs. In this respect, we predict that both the electronic and optical gaps of ZnSe QDs scale nearly linearly with the inverse diameter [cf. Table I and Fig. 2(c)], while, for ZnS QDs, the size-dependent scaling of the electronic or optical gaps resembles much their CdSe counterparts, with $\gamma_{\mathrm{ZnS}} = 1.23$ and $\gamma_{\mathrm{ZnS}}^X = 1.44$, respectively [cf. Table I and Fig. 2(d)].

It is worthwhile to compare our *ab initio* results with those obtained based on various commonly applied tight binding models concerning the material systems of interest herein, including the sp^3s^* model [or reduced $s_c p_a^3$ model (Refs. [41,42])] and the sp^3d^5 model (Refs. [43,44]), which shall be useful for the development of the more sophisticated TB model [cf. Figs. 2(a)–2(d)]. We find that, for CdSe and CdS QDs, the sp^3s^* model or even the reduced $s_c p_a^3$ model delivers electronic gaps (i.e., without considering excitonic effects) that are in good agreement with our B3LYP results [cf. Figs. 2(a) and 2(b)]. However, when it comes to ZnS QDs, the sp^3s^* model seems to significantly underestimate (>1 eV at QD diameter around 1 nm) the single-particle gap in comparison to our *ab initio* results. Removing the S^* orbital but including the d orbital in the tight-binding model, that is, the sp^3d^5 model, does not seem to improve significantly the results [cf. Fig. 2(d)]. This remains the case for ZnSe QDs [cf. Fig. 2(c)]. Based on those comparisons, a possible way of resolving the discrepancy between TB results and the current *ab initio* results is to further increase the size of the basis set, e.g., the $sp^3d^5s^*$ model, and simultaneously account for the second-nearest-neighbor interactions. However, to the best of our knowledge, the TB parametrizations of the $sp^3d^5s^*$ model have only been made on bulk CdSe of the zinc-blende structure [48], and the size-dependent evolution of the electronic gap remains unavailable for comparisons. Therefore, further development on the TB model would require careful and reliable parametrizations of the $sp^3d^5s^*$ model, subsequently applying it to QD material systems, including particularly those heavy-metal free ones, such as ZnSe and ZnS QDs.

QD stoichiometry is found to have marginal impact on the size-dependent scaling of both electronic and optical gaps. Indeed, $\alpha = 4.30$ and $\beta = 1.23$ for off-stoichiometric CdSe QDs with T_d point group symmetry. Those values reduce slightly to $\alpha = 4.09$ and $\beta = 1.17$ for stoichiometric QD with lowered C_{3v} point group symmetry. Remarkably, we find that the HOMO state of the stoichiometric QD switches its symmetry character from a Γ_{3v} symmetry to a Γ_{1v} symmetry when enhancing quantum confinement effects. The critical diameter is found to be around 1 nm for all QD systems. This results in a drastic change in the optical polarization at the lower part of the absorption spectra [cf. Figs. 3(a) and 3(b)]. Before the switch, the lowest bright exciton state exhibits a Γ_{3v} symmetry ($\Gamma_{3v} \otimes \Gamma_{1c} = \Gamma_3^{\mathrm{X}}$) and is circularly polarized [i.e., along the (x, y)–in plane direction; cf. Fig. 3(a)]. However, after the switch, the lowest bright exciton state appears to be of Γ_1 symmetry ($\Gamma_{1v} \otimes \Gamma_{1c} = \Gamma_1^{\mathrm{X}}$) and linearly polarized exclusively along the z direction [cf. Fig. 3(b)]. Such linear polarization of a near-band-edge exciton state has commonly been realized in nanostructures of group II-VI with wurtzite structure, such as CdSe nanorods [49], ZnO QDs under hydrostatic pressure [23], CdSe dot-in-rod [50], and ZnO and GaN nanowires [51,52]. However, it has been rarely observed in QDs of group II-VI with zinc-blende structure. Stoichiometric control combined with enhanced quantum confinement effects thus serve as an enabling means of realizing linearly polarized emission in QDs of zinc-blende structure, which is highly appealing for polarized light emitting diodes and quantum information science and technologies.

Exciton lifetime as a function of QD size for all material systems is studied in Fig. 3(c). It is shown that the exciton lifetime obtained in the current theoretical scheme appears in a nanosecond time scale and increases monotonically with increasing the QD diameter [cf. Fig. 3(c)], which is in excellent agreement with experiment for CdSe QDs [54]. Strikingly, the size-dependent lifetime is found to be inversely proportional to the QD diameter and tends to saturate at larger size. This is justified by the fact that the numerical data can be well fitted with the formula $\tau = \tau_\infty + \beta/D$, where τ_∞ represents the exciton decay lifetime at the bulk limit and β is a proportionality constant. The obtained fitting parameters are compiled in Table II. It is found that τ_∞ decreases when the band gap energy of the corresponding bulk material increases. Indeed, $\tau_{\mathrm{CdSe},\infty} \approx 2\tau_{\mathrm{CdS},\infty} \approx 3\tau_{\mathrm{ZnSe},\infty} \approx 5\tau_{\mathrm{ZnS},\infty}$. β is found to be mostly negative. It also decreases (in absolute value) with increase of the band gap energy of corresponding bulk material, i.e., $\beta_{\mathrm{CdSe}} > \beta_{\mathrm{CdS}} > \beta_{\mathrm{ZnSe}} > \beta_{\mathrm{ZnS}}$ (cf. Table II). Particularly, we find that the exciton lifetime of ZnS QD appears insensitive to the quantum confinement effects, exhibiting a nearly vanishing β value [cf. Table II and Fig. 3(c)]. We note that the exciton decay lifetime not only depends on the QD size but also is highly sensitive to the QD stoichiometry, surface chemistry, and particularly thermal noise.

The singlet-triplet splitting Δ_{ST}, defined as the energy difference between the lowest spin-singlet and spin-triplet exciton states (cf. Fig. 1), is studied as a function of the QD size in Fig. 3(d). We find that Δ_{ST} of CdSe QDs appears comparable to that of CdS QDs at a given QD size, and turns out to be considerably larger than that of ZnSe and ZnS QDs [cf. Fig. 3(d)]. This is particularly true when enhancing quantum confinement effects. The magnitude of Δ_{ST} is determined by the strength of the exchange coupling between the electron and hole states involved in forming the ground-state exciton manifold, which in turn depends strongly on the spatial wave function overlapping between them. Indeed, compared to ZnSe and ZnS QDs, CdSe and CdS counterparts, which have the largest ratios between the electron and hole effective masses in bulk phases (cf. Table II)

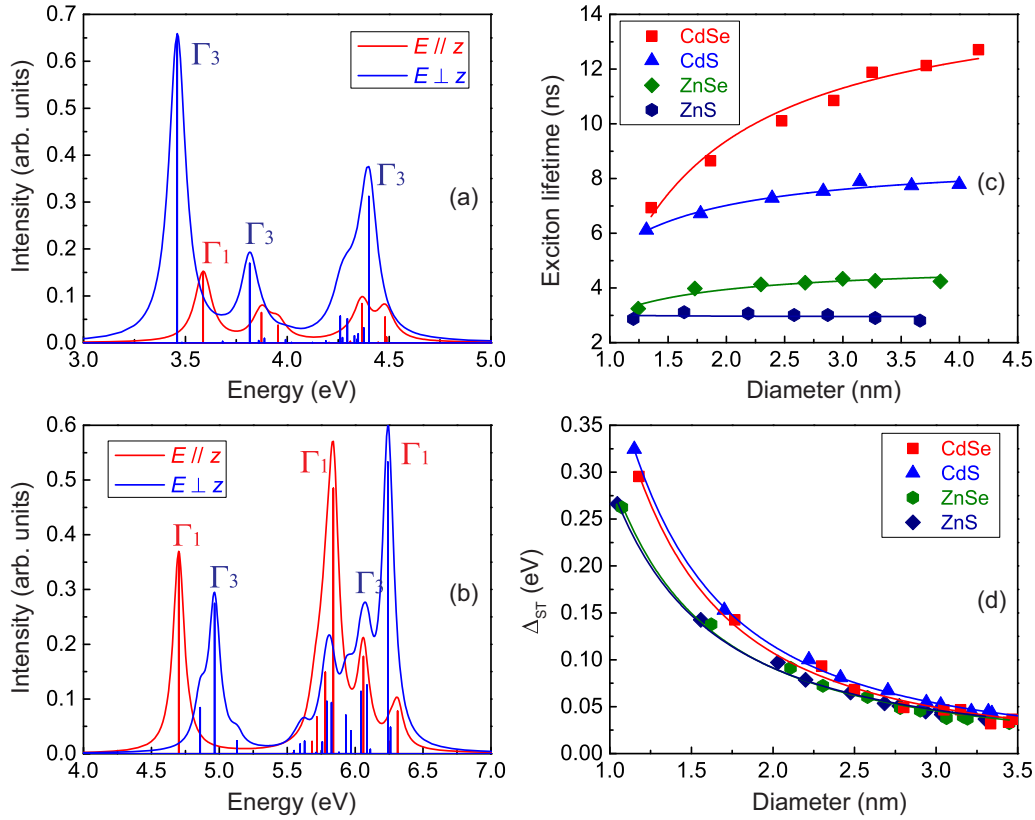

FIG. 3. (a), (b) Optical absorption of colloidal stoichiometric CdSe quantum dots with sizes (a) $D = 1.77$ nm and (b) 1.18 nm, respectively. The vertical lines in each plot show the absorption peak corresponding to each exciton state. The symmetry character corresponding to the pronounced absorption peak is labeled alongside. (c) Radiative exciton decay lifetime and (d) singlet-triplet splitting as a function of the diameter of off-stoichiometric CdSe, CdS, ZnSe, and ZnS quantum dots. Each solid line represents a fit to the numerical data (see main text for details).

and therefore the strongest electron-hole overlapping, exhibit the largest Δ_{ST}. Furthermore, the size-dependent singlet-triplet splitting is found to scale as $\Delta_{\mathrm{ST}} = \Delta_{\mathrm{ST},\infty} + 1/D^{\delta}$, with $\Delta_{\mathrm{ST},\infty}$ being the extrapolated singlet-triplet splitting at the bulk limit and δ being a fitting parameter [cf. Fig. 3(d)]. We find that our extrapolated single-triplet exchange splitting of bulk ZnSe $\Delta_{\mathrm{ST},\infty}^{\mathrm{ZnSe}} = 0.3$ meV, which is in fair agreement with the experimental value of 0.45 meV [55,56]. For CdSe of zinc-blende structure, our extrapolated value $\Delta_{\mathrm{ST},\infty}^{\mathrm{CdSe}} = 0.41$ meV. The experimental value is 0.13 meV [57,58] and the theoretical value for bulk CdSe of wurtzite structure based on the local-density approximation pseudopotential method is 0.04978 meV [58]. One possible way of further resolving the discrepancy between theory and experiment is to employ the recently developed triplet tuning technique based on a range-separated density functional [59]. Remarkably, the resultant δ value is found to be close to 2 for CdSe QDs, and it decreases when the band gap energy of the corresponding bulk material increases, i.e., $\delta_{\mathrm{CdSe}} > \delta_{\mathrm{CdS}} > \delta_{\mathrm{ZnSe}} > \delta_{\mathrm{ZnS}}$ (cf. Table II).

C. Ligand effects

After exploring the size-dependent excitonic characteristic of QDs of group II-VI using a simple pseudohydrogen passivation scheme, we put forth the study of surface ligand effects introduced by passivation of QD with halogen, such

TABLE II. Compiled electron (m_e^*) and heavy hole (m_{hh}^*) effective masses of bulk CdSe, CdS, ZnSe, and ZnS. The obtained fitting parameters of τ_∞, $\Delta_{\mathrm{ST},\infty}$, β, and δ for CdSe, CdS, ZnSe, and ZnS quantum dots obtained from current hybrid time-dependent hybrid time-dependent density functional theory. The effective masses (in units of m_0) are taken from Ref. [53].

	Effective mass (m_0)		Lifetime (ns)		Δ_{ST} (meV)	
Materials	m_e^*	m_{hh}^*	τ_∞	β	$\Delta_{\mathrm{ST},\infty}$	δ
CdSe	0.11	0.33	15.17	−11.60	0.41	1.93
CdS	0.14	0.39	8.78	−3.53	0.42	1.87
ZnSe	0.12	0.52	4.88	−1.87	0.30	1.72
ZnS	0.20	0.96	2.93	0.08	0.29	1.66

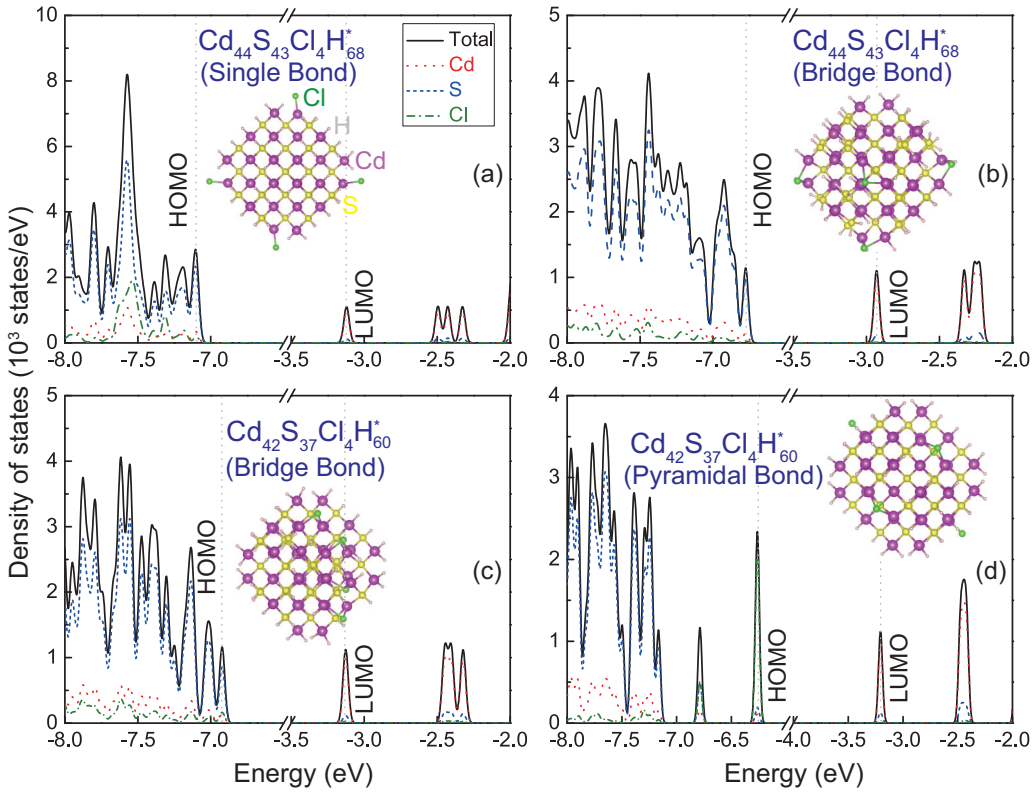

FIG. 4. Atom resolved density of states of chlorine-containing CdS quantum dots with solely (a) Cd-Cl single bond, (b) Cd-Cl-Cd bridge bond between two doubly coordinated surface Cd atoms, (c) Cl-Cd-Cl bridge bond between two triply coordinated surface Cd atoms, and (d) mixed single and trigonal pyramidal bonds, respectively. The inset shows the corresponding optimized geometric structure with specific bonding configuration.

as chloride (Cl). Indeed, chloride post-treatment of QDs introduced through the liquid or solid ligand exchange process has recently shown to significantly improve the luminescence quantum yield and achieve the best ever performance of blue-emitting devices of group II-VI [3]. Moreover, short inorganic ligand is also beneficial for the reduction of interdot distance in the solid-state QD film, therefore enhancing the wave-function overlap between the neighboring dots and facilitating the charge transport. The emphasis herein is placed on the exploration of the surface passivation mechanism and optical signature of chloride decoration compared with the commonly applied fully pseudohydrogen passivation scheme.

We take CdS QDs as a prototype system, and focus exclusively on the chloride ligand binding to the cation Cd atoms, which have been experimentally confirmed under a cation rich condition. Two types of surface Cd atoms are considered, i.e., doubly coordinated surface Cd atom and triply coordinated surface Cd atom. The former type corresponds to the surface Cd atom coordinating only with two inner sulfur atoms ("doubly coordinated") and leaving with two unpassivated surface bonding bonds with a fractional charge of $1/2$ each in accordance with the electron counting model. The latter type corresponds to the surface Cd atom coordinating with three inner sulfur atoms ("triply coordinated") and leaving with only one dangling bond with a fractional charge of $1/2$. The chloride-decorated QDs are created by replacing some of the pseudohydrogen atoms with chloride passivants. A side-by-side comparison of the electronic structures and excitonic properties between the fully pseudohydrogen passivated QDs and the chloride decorated counterparts allows one to quantify the impact of surface ligand.

We first identify the most favorable bonding configuration employing the electron counting model and subsequent quantum mechanical checkup calculations by continuously monitoring the bond formation between the passivant and the absorbate. By such a way, three bonding configurations have been explored, i.e., Cd-Cl single bond, Cd-Cl-Cd bridging bond, and Cl-Cd_3 NH_3-like trigonal pyramidal bond. The single bond appears when one chloride atom binds with a doubly coordinated surface Cd atom [cf. Fig. 4(a)]. Each involved atom fulfills the eight-valence electron rule and the QD maintains charge neutrality. In such a bonding configuration, the surface state induced by the dangling bond is pushed far below the HOMO state. The resultimg HOMO state has a nearly pure contribution from the p orbital of sulfur atoms [cf. Fig. 4(a)], recovering the situation of fully pseudohydrogen passivated QD. A similar situation can be reached when one chloride atom connects to two neighboring doubly coordinated surface Cd atoms, forming a bridgelike bond ("bridging bond") but leaving the other dangling bond on each Cd atom pseudohydrogen passivated [cf. Fig. 4(b)]. Comparing with the single bond, the bond length between the Cd and Cl atoms $d_{\mathrm{Cd-Cl}}$ of

the bridge bond is considerably elongated. $d_{Cd-Cl} = 2.36$ Å for the single bond, and it appears to be over 10% larger for a bridge bond.

Concerning the passivation of triply coordinated surface Cd atoms, two passivating schemes have been explored. The first scheme is that one chloride atom binds with two neighboring triply coordinated surface Cd atoms, therefore forming a bridge bond [cf. Fig. 4(c)]. Such a bonding configuration appears very much like the bridge bond formed between two doubly coordinated surface Cd atoms but without involving further pseudohydrogens. Indeed, d_{Cd-Cl} for both types of bridge bonds turns out to be nearly the same, i.e., $d_{Cd-Cl} \approx 2.6$ Å. The resultant density of states plots are shown in Fig. 4(c). It is found that such a passivation scheme also pushes the surface state far below the HOMO state, again recovering a similar situation as the pseudohydrogen passivation scheme at the band edges. The other passivation scheme regarding the triply coordinated surface Cd atoms involves simultaneously two chloride atoms. One of the chloride atoms connects with three triply coordinated surface Cd atoms, forming a NH_3-like trigonal pyramidal bond, while the other chloride atom binds with one additional triply coordinated surface Cd atom, forming a single bond [cf. Fig. 4(d)]. In the trigonal pyramidal bonding configuration, the Cl atom takes 1/3 fractional electron from each bonded surface Cd atom, reproducing the bonding configuration in bulk $CdCl_2$. Indeed, d_{Cd-Cl} in the trigonal pyramidal bonding configuration appears as $d_{Cd-Cl} = 2.76$ Å, which is nearly the same as in the $CdCl_2$ bulk phase (∼2.68 Å). In comparison, d_{Cd-Cl} in the single bond is much shorter (∼2.38 Å), but appears the same as its counterpart that passivates a doubly coordinated surface Cd atom. We note that such a passivation scheme requires concurrently forming both a trigonal pyramidal bond and a single bond. Neither the trigonal pyramidal bond nor the single bond independently enable a perfect passivation, because of the violation of the eight-valence electron rule and charge neutrality.

We next examine the electronic structure and excitonic optical property of chloride-decorated QDs with the aforementioned passivation schemes in comparison with those of the fully pseudohydrogen passivated counterpart. It is found that chloride decoration serves as a hole delocalization ligand. The charge density of the HOMO state tends to deplete from the center of the QD and accumulate towards the surface. Consequently, the HOMO-LUMO electronic gap decreases with increasing the chloride concentration, compared with that of fully pseudohydrogen passivated QD. For our smallest sized off-stoichiometric CdS QD, we find that the reduction in the electronic gap can be as large as 1.44 eV for a fully chloride passivated QD ($Cd_{16}S_{13}Cl_{12}H^*_{12}$) in comparison to a fully pseudohydrogen passivated counterpart (e.g., $Cd_{16}S_{13}H^*_{36}$, not shown).

The delocalization of the hole state and the reshaping of the density of states because of chloride passivation have caused significant impact on the excitonic properties of the QD (cf. Fig. 5). Comparing with fully pseudohydrogen passivated QD, four distinct optical characteristics induced by chloride decoration have been explored. (i) Redshifted absorption spectra. Such a redshift enhances with increase of the chloride concentration, irrespective of the bonding configurations. (ii) Reduced absorption intensity, at least at the lower part of the spectra, being mainly caused by delocalization of the hole states. Interestingly, we find that the reduction in the absorption intensity is more pronounced when forming a bridge bond compared to QDs with only Cd-Cl single bond configuration [cf. Figs. 5(a)–5(c)]. Indeed, the oscillator strength of the first bright exciton state f_{osc}, being contributed dominantly from the HOMO-LUMO transition, appears to be 0.343 in velocity representation (without any symmetry constraint) for a chloride-free QD with a size around 1.7 nm (e.g., $Cd_{43}S_{40}H^*_{72}$). However, it reduces to $f_{osc} = 0.18$ when forming only one bridge bond between two triply coordinated surface Cd atoms, because of decreased electron-hole wave function overlapping and therefore reduced dipole moment. The oscillator strength further reduces to $f_{osc} = 0.08$ when increasing the number of bridge bonds to four. In contrast, the oscillator strength only slightly decreases to $f_{osc} = 0.29$ when forming four single bonds at the surface of the same QD. (iii) Comparing with bridge bond configuration, QDs with mixed single and triangular pyramid bond configuration exhibit the most pronounced redshift and reduction in the absorption spectrum [cf. Figs. 5(d)–5(f)]. Particularly, the reduction in the oscillator strength in the first optically bright exciton state can reach up to a few orders of magnitude smaller, which is essentially the dark state, due to the trap nature of the involved hole states [cf. inset of Fig. 5(f)]. (iv) Enhanced exciton decay lifetime, irrespective of chloride concentration and bonding configurations. Again, we find that the increase in exciton lifetime is more pronounced for QDs with bridge bond configuration. Indeed, chloride-decorated QDs with only four bridge bonds deliver an exciton decay lifetime (∼97.7 ns) being over five times that in the corresponding pseudohydrogen passivated QD (∼19.25 ns). We note that the enhancement of exciton decay time can reach up to a few orders of magnitude larger in QD with mixed single and triangular pyramid bond configuration. For example, $Cd_{42}S_{37}Cl_4H^*_{60}$ QD with two pairs of mixed bonds exhibits a decay time reaching up to 0.43 ms, suggesting that the first optically allowed exciton state is essentially dark.

IV. CONCLUSION

To summarize, we have studied the electronic and excitonic properties of colloidal quantum dots (QDs) of group II-VI with realistic sizes, including CdSe, CdS, ZnSe, and ZnS QDs. It is found that the calculated optical gaps of all types of QDs are in excellent quantitative agreement with experiment using the hybrid time-dependent density functional theory. Based on the calculated numerical results, scaling laws of size-dependent energy gaps governed solely by quantum confinement effects have been explored at both single-particle level and correlated excitonic level for all QDs. Interestingly, the single-particle gap of ZnSe QDs appears to scale nearly linearly as a function of the inverse diameter, and such a scaling is slightly softened by accounting for the excitonic effects. We have predicted an electronic state crossover whereby the nature of the highest occupied molecular orbital (HOMO) state switches its symmetry from Γ_3 to Γ_1 at a diameter around 1 nm for all QDs upon stoichiometric control and quantum confinement effects. After the switching, the pronounced

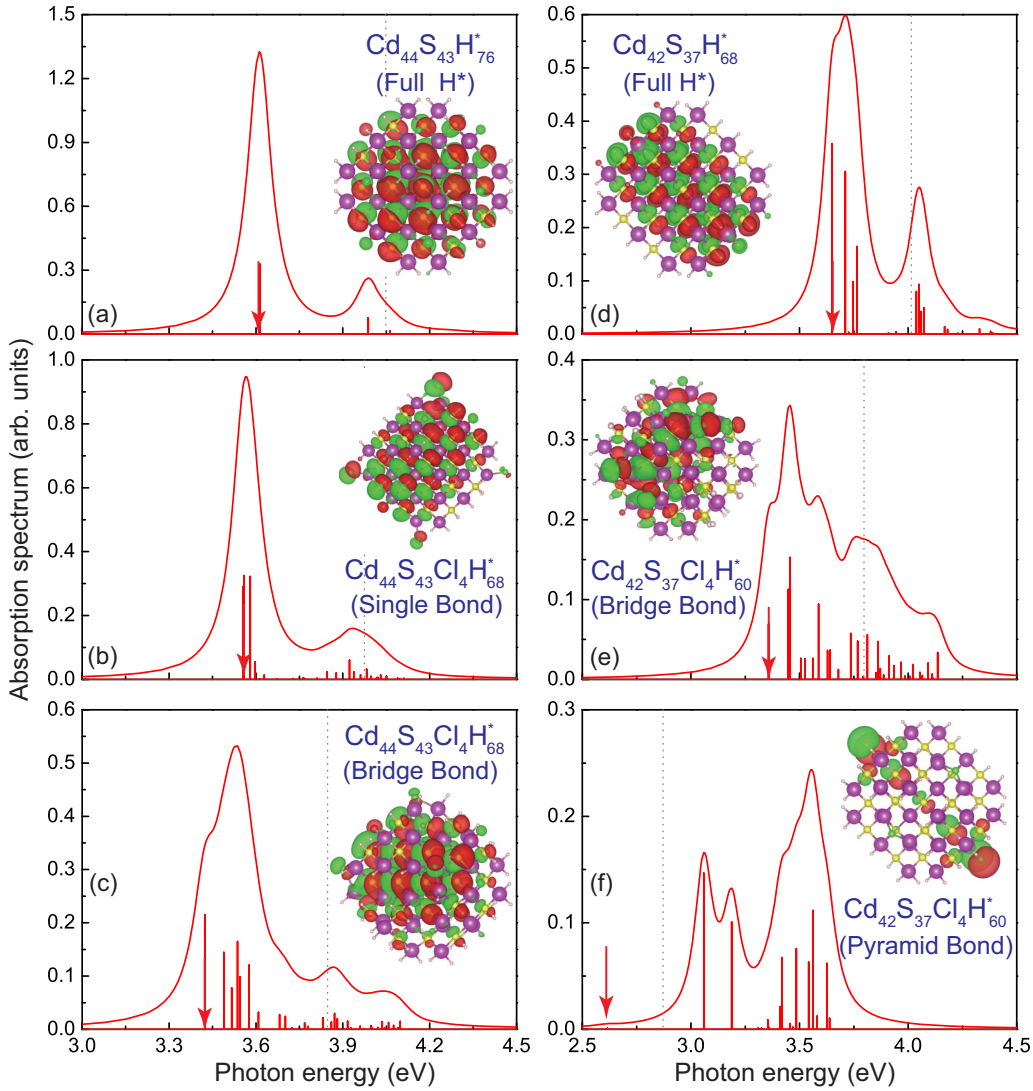

FIG. 5. Absorption spectrum of (a), (d) solely pseudohydrogen passivated and (b), (c) and (e), (f) pseudohydrogen and chlorine copassivated CdS quantum dots with only (b) Cd-Cl single bond, (c) Cd-Cl-Cd bridge bond between two doubly coordinated surface atoms, (e) Cd-Cl-Cd bridge bond between two triply coordinated surface atoms, and (f) mixed single and trigonal pyramidal bonds, respectively. Two dot sizes are considered, i.e., $Cd_{44}S_{43}H^*_{76}$, and $Cd_{92}S_{83}H^*_{116}$, respectively. Each spectra is obtained by calculating 30 optically bright singlet exciton states and using a Lorentzian broadening function with broadening parameter $\Gamma = 0.05$ eV. The vertical lines in each plot show the absorption peak corresponding to each exciton state. The vertical arrow and gray dashed line in each plot indicate the optical gap and HOMO-LUMO electronic gap, respectively. The inset shows the charge density of the HOMO state of the corresponding quantum dot system.

band-edge exciton state appears linearly polarized with the polarization direction exclusively along the z direction. The radiative exciton decay lifetime for all QDs is found to increase monotonically with increase of the QD size but tends to saturate at larger sizes, following a $1/D$ scaling law, where D is the diameter of the QD. The exciton lifetime appears highly dependent on the nature of the QD material, and decreases with increase of the band gap energy of the corresponding bulk material.

On the grounds of the electron counting model and quantum mechanical calculations using hybrid density functional theory, we have also explored the passivation mechanisms of inorganic chloride ligand, and associated impacts on the electronic and excitonic properties of colloidal QDs of group II-VI. For doubly coordinated surface Cd atoms, the surface dangling bonds can be effectively passivated by forming Cd-Cl single bonds. While, for triply coordinated surface Cd atoms, two passivation schemes have been identified. The first scheme is achieved by forming a Cl-Cd-Cl bridging bond with one chloride surface passivant shared by two neighboring Cd absorbates. The other scheme simultaneously involves two chloride surface passivants with one of them coordinating with three Cd surface absorbates forming a NH_3-like trigonal pyramidal bond and the other one connecting with an additional triply coordinated surface Cd atom forming a Cd-Cl single bond. For all types of bonding configurations, chloride ligand serves as a hole delocalization ligand and tends to redshift the absorption spectra and reduce the absorption intensity, at least at the lower part of the spectra. The exciton decay lifetime experiences significant enhancement because

of reduced electron-hole wave function overlapping, reaching up to a few magnitudes depending on the bonding configurations. The results presented herein are not only interesting from the fundamental physics point of view for gaining insight into the excitonic characteristics, but also are technologically important for the development of optoelectronic devices based on colloidal QDs of group II-VI.

ACKNOWLEDGMENTS

The work has been partly supported by the NSFC project with Grants No. 11804077 and No. 11774078, and partly by the innovation research team of science and technology in Henan province (20IRTSTHN020). Z.Z. acknowledges the support of the Distinguished Professor grant of Henan University with Grant No. 2018001T.

[1] Y.-H. Won, O. Cho, T. Kim, D.-Y. Chung, T. Kim, H. Chung, H. Jang, J. Lee, D. Kim, and E. Jang, Nature (London) **575**, 634 (2019).
[2] H. Shen, Q. Gao, Y. Zhang, Y. Lin, Q. Lin, Z. Li, L. Chen, Z. Zeng, X. Li, Y. Jia, S. Wang, Z. Du, L. S. Li, and Z. Zhang, Nat. Photon. **13**, 192 (2019).
[3] T. Kim, K.-H. Kim, S. Kim, S.-M. Choi, H. Jang, H.-K. Seo, H. Lee, D.-Y. Chung, and E. Jang, Nature (London) **586**, 385 (2020).
[4] O. Chen, J. Zhao, V. P. Chauhan, J. Cui, C. Wong, D. K. Harris, H. Wei, H.-S. Han, D. Fukumura, R. K. Jian, and M. G. Bawendi, Nat. Mater. **12**, 445 (2013).
[5] X. Dai, Y. Deng, X. Peng, and Y. Jin, Adv. Mater. **29**, 1607022 (2017).
[6] H. Moon, C. Lee, W. Lee, J. Kim, and H. Chae, Adv. Mater. **31**, 1804294 (2019).
[7] T. Cheng, Z. Wang, S. Jin, F. Wang, Y. Bai, H. Feng, B. You, Y. Li, T. Hayat, and Z. Tan, Adv. Opt. Mater. **5**, 1700035 (2017).
[8] H. Jia, F. Wang, and Z. Tan, Nanoscale **12**, 13186 (2020).
[9] F. Chen, Q. Lin, H. Shen, and A. Tang, Mater. Chem. Front. **4**, 1340 (2020).
[10] E. Jang, Y. Kim, Y.-H. Won, H. Jang, and S.-M. Choi, ACS Energy Lett. **5**, 1316 (2020).
[11] C. Xiang, W. Koo, S. Chen, F. So, X. Liu, X. Kong, and Y. Wang, Appl. Phys. Lett. **101**, 053303 (2012).
[12] A. Wang, H. Shen, S. Zang, Q. Lin, H. Wang, L. Qian, J. Niu, and L. Song Li, Nanoscale **7**, 2951 (2015).
[13] E.-P. Jang, C.-Y. Han, S.-W. Lim, J.-H. Jo, D.-Y. Jo, S.-H. Lee, S.-Y. Yoon, and H. Yang, ACS Appl. Mater. Interfaces **11**, 46062 (2019).
[14] L. Qian, Y. Zheng, J. Xue, and P. H. Holloway, Nat. Photon. **5**, 543 (2011).
[15] H. Shen, W. Cao, N. T. Shewmon, C. Yang, L. S. Li, and J. Xue, Nano Lett. **15**, 1211 (2015).
[16] Y. M. Niquet, C. Delerue, G. Allan, and M. Lannoo, Phys. Rev. B **62**, 5109 (2000).
[17] M. Zielinski, Phys. Rev. B **86**, 115424 (2012).
[18] S. Lee, L. Jönsson, J. W. Wilkins, G. W. Bryant, and G. Klimeck, Phys. Rev. B **63**, 195318 (2001).
[19] L.-W. Wang and A. Zunger, Phys. Rev. B **53**, 9579 (1996).
[20] A. Franceschetti, H. Fu, L. W. Wang, and A. Zunger, Phys. Rev. B **60**, 1819 (1999).
[21] S. Baskoutas and G. Bester, J. Phys. Chem. C **114**, 9301 (2010).
[22] Z. Zeng, C. S. Garoufalis, S. Baskoutas, and G. Bester, Phys. Rev. B **87**, 125302 (2013).
[23] Z. Zeng, C. S. Garoufalis, S. Baskoutas, Y. Jia, and G. Bester, Phys. Rev. B **98**, 235410 (2018).
[24] X. Ma, J. Min, Z. Zeng, C. S. Garoufalis, S. Baskoutas, Y. Jia, and Z. Du, Phys. Rev. B **100**, 245404 (2019).
[25] O. I. Micic, H. M. Cheong, H. Fu, A. Zunger, J. R. Sprague, A. Mascarenhas, and A. J. Nozik, J. Phys. Chem. B **101**, 4904 (1997).
[26] O. Micic and A. Nozik, J. Lumin. **70**, 95 (1996).
[27] E. Cho, H. Jang, J. Lee, and E. Jang, Nanotechnology **24**, 215201 (2013).
[28] TURBOMOLE V7.3 2018, a development of University of Karlsruhe and Forschungszentrum Karlsruhe GmbH, 1989-2007, TURBOMOLE GmbH, since 2007; available from http://www.turbomole.com.
[29] J. P. Perdew, K. Burke, and M. Ernzerhof, Phys. Rev. Lett. **77**, 3865 (1996).
[30] P. J. Stephens, F. J. Devlin, C. F. Chabalowski, and M. J. Frisch, J. Phys. Chem. **98**, 11623 (1994).
[31] F. Weigend and R. Ahlrichs, Phys. Chem. Chem. Phys. **7**, 3297 (2005).
[32] F. Weigend, Phys. Chem. Chem. Phys. **8**, 1057 (2006).
[33] D. L. Dexter, Solid State Phys. **6**, 353 (1958).
[34] L. Zhang, J.-W. Luo, A. Franceschetti, and A. Zunger, Phys. Rev. B **84**, 075404 (2011).
[35] J. Jasieniak, M. Califano, and S. E. Watkins, ACS Nano **5**, 5888 (2011).
[36] R. W. Meulenberg, J. R. Lee, A. Wolcott, J. Z. Zhang, L. J. Terminello, and T. van Buuren, ACS Nano **3**, 325 (2009).
[37] T. Vossmeyer, L. Katsikas, M. Giersig, I. G. Popovic, K. Diesner, A. Chemseddine, A. Eychmueller, and H. Weller, J. Phys. Chem. **98**, 7665 (1994).
[38] J. Maes, N. Castro, K. De Nolf, W. Walravens, B. Abécassis, and Z. Hens, Chem. Mater. **30**, 3952 (2018).
[39] L. Yang, R. Xie, L. Liu, D. Xiao, and J. Zhu, J. Phys. Chem. C **115**, 19507 (2011).
[40] J. Nanda, S. Sapra, D. D. Sarma, N. Chandrasekharan, and G. Hodes, Chem. Mater. **12**, 1018 (2000).
[41] P. E. Lippens and M. Lannoo, Phys. Rev. B **39**, 10935 (1989).
[42] S. Schulz and G. Czycholl, Phys. Rev. B **72**, 165317 (2005).
[43] S. Sapra and D. D. Sarma, Phys. Rev. B **69**, 125304 (2004).
[44] J. G. Díaz, M. Zieliński, W. Jaskólski, and G. W. Bryant, Phys. Rev. B **74**, 205309 (2006).
[45] C. Ullrich, *Time-Dependent Density-Functional Theory: Concepts and Applications* (Oxford University Press, Oxford, 2012).
[46] L. E. Brus, J. Chem. Phys. **80**, 4403 (1984).
[47] J. Li and L.-W. Wang, Phys. Rev. B **72**, 125325 (2005).
[48] E. Kalesaki, W. H. Evers, G. Allan, D. Vanmaekelbergh, and C. Delerue, Phys. Rev. B **88**, 115431 (2013).
[49] J. Hu, L.-s. Li, W. Yang, L. Manna, L.-w. Wang, and A. P. Alivisatos, Science **292**, 2060 (2001).
[50] J. Planelles, F. Rajadell, and J. I. Climente, J. Phys. Chem. C **120**, 27724 (2016).

[51] Z. Zeng, A. Petoni, C. S. Garoufalis, S. Baskoutas, and G. Bester, Phys. Chem. Chem. Phys. **17**, 1197 (2015).
[52] A. Molina-Sánchez, A. García-Cristóbal, and G. Bester, Phys. Rev. B **86**, 205430 (2012).
[53] S. Adachi, *Handbook on Physical Properties of Semiconductors* (Kluwer Academic Publishers, Dordrecht, 2004).
[54] Y. Gao and X. Peng, J. Am. Chem. Soc. **137**, 4230 (2015).
[55] O. Madelung and Landolt-Bornstein, *Numerical Data and Functional Relationships in Science and Technology, Series III, Vols. 17a, 17b, 22a, and 41b* (Springer, Berlin, 1999).
[56] M. Cardona, T. Ruf, and J. Serrano, Phys. Rev. Lett. **86**, 3923 (2001).
[57] V. A. Kiselev, B. S. Razbirin, and I. N. Uraltsev, Phys. Status Solidi B **72**, 161 (1975).
[58] H. Fu, L.-W. Wang, and A. Zunger, Phys. Rev. B **59**, 5568 (1999).
[59] Z. Lin and T. Van Voorhis, J. Chem. Theory Comput. **15**, 1226 (2019).